RSC Advances

PAPER

View Article Online
View Journal | View Issue

Cite this: *RSC Adv.*, 2022, **12**, 20191

Effect of concentration of glycidol on the properties of resorcinol-formaldehyde aerogels and carbon aerogels†

Xiurong Zhu, *[abc] Lousia J. Hope-Weeks,*[b] Yi Yu,[a] Jvjun Yuan,[a] Xianke Zhang,[a] Huajun Yu,[a] Jiajun Liu,[a] Xiaofen Li[a] and Xianghua Zeng[a]

Received 25th May 2022
Accepted 6th July 2022

DOI: 10.1039/d2ra03270h

rsc.li/rsc-advances

By using glycidol as a catalyst, high porosity, low-density resorcinol (R) and formaldehyde (F) aerogels and carbon aerogels (CAs) were synthesized *via* a sol-gel method. The effect of glycidol and water on the color, density, morphology, textual characteristics and adsorption properties of the resultant RF aerogels and CAs were investigated in detail. The results revealed that the properties of RF aerogels and CAs can be controlled by adjusting the amount of glycidol and water. The resultant RF aerogels and CAs were porous materials, the minimum densities of RF aerogels and CAs were 96 and 110 mg cm^{-3} respectively while the maximum specific surface areas of RF aerogels and CAs were 290 and 597 m^2 g^{-1}. The maximum adsorption capacity of CAs was about 125 mg g^{-1} on Rhodamine B, which was higher than that of some reported CAs catalyzed by base and acid catalysts. The sol-gel mechanisms of RF aerogels and CAs can be attributed to the opening of the epoxy group of glycidol in the mixture of R and F.

1 Introduction

Due to their controllable density and nano-scale homogeneous microstructure, aerogels possess interesting chemical and physical properties, such as ultra-low density, ultra-high specific surface area, ultra-high porosity, ultralow thermal conductivity and so on.[1] In recent years, many researchers have focused on the investigation of SiO_2 aerogels,[2] resorcinol (R)-formaldehyde (F) aerogels and carbon aerogels (CAs),[3,4] graphene aerogels,[5,6] 3D MoS_2 aerogels[7] and so on.

Pekala *et al.* first reported the synthesis of porous RF aerogels and CAs *via* the hydrolysis and polycondensation of R with F.[8,9] Due to their fascinating physiochemical properties, including low density, large surface area and continuous porosity, RF aerogels and CAs have been increasingly investigated in recent years and widely used in a variety of areas, such as catalyst supports,[10–12] adsorbents,[13,14] supercapacitors,[15,16] battery electrodes,[17,18] thermal insulation[19] and 3D printable ink.[20–23]

To obtain RF aerogels and CAs, the addition/polymerization reactions of R and F are always catalyzed by base and acidic catalysts.[24–26] In the case of base catalysts (*e.g.*, Na_2CO_3,[27] $NaHCO_3$,[28] NaOH,[29] K_2CO_3,[30] $KHCO_3$,[28] $Ca(OH)_2$),[31] the R is firstly deprotonated to form R anions, which can react with F through an addition reaction, giving rise to hydroxymethyl derivatives. Whereas the acid is used as catalysts (*e.g.*, *para*-toluenesulfonic acid,[32] acetic acid,[33] picric acid,[34] salicylic acid,[35] citric acid,[36] hydrochloric acid,[37,38] cetyltrimethylammonium bromide,[39] *m*-hydroxybenzoic,[40] gallic acid,[40] oxalic acid,[32,40] succinic acid,[40] benzoic acids[41] and hexamethylenetetramine[42]), the F is firstly protonated and then reacts with R to produce hydroxymethyl derivatives. Both derivatives derived from base or acidic catalysts undergo a polymerization reaction to form methylene and methylene ether bridged compounds, and then clusters, colloidal particles, wet RF gels.[3] The wet RF gels are solvent-substituted and then dried to form RF aerogels. The CAs can be obtained by pyrolyzing of RF aerogels. Many factors, such as the catalyst type and concentration, concentrations of the main ingredients (R and F), initial solution pH, curing time and temperature, can strongly effect the properties of the ultimate RF aerogels and CAs.[43,44]

Due to the poor mechanical properties of pristine CAs derived from base and acidic catalysts, glycidol have been used as catalyst to enhance the compressive strengths of CAs. The maximum compressive strength of glycidol-catalyzed CAs was 2.55 MPa (at the density of 187 mg cm^{-3} and specific surface area of 580 m^2 g^{-1}), which are higher than that of other reported pristine CAs with similar bulk density. The sol-gel mechanisms of glycidol-catalyzed CAs and improvement

[a]*School of Physics and Electronic Information, Gannan Normal University, Ganzhou, Jiangxi, 341000, China. E-mail: zxr20786@gnnu.edu.cn; zxr20786@hotmail.com; Tel: +86 18379889420*

[b]*Department of Chemistry and Biochemistry, Texas Tech University, Lubbock, Texas, 79409, USA. E-mail: louisa.hope-weeks@ttu.edu; Tel: +1 8068342442*

[c]*Shanghai Key Laboratory of Special Artificial Microstructure Materials & Technology, Department of Physics, Tongji University, Shanghai 200092, China. Tel: +86 18379889420*

† Electronic supplementary information (ESI) available. See https://doi.org/10.1039/d2ra03270h

of mechanical properties were likely attributed to the ring-opening of epoxy group of glycidol in the mixture of R and F,[3] which are not consistent with that of base and acidic catalysts.

However, to our best knowledge, there is no study on the effect of concentration of glycidol on the color, density, morphology, composition, textual characteristics and adsorption properties of the glycidol-catalyzed RF aerogels and CAs. Herein, the evolution of color, density, morphology, composition, textual characteristics and adsorption properties of the glycidol-catalyzed RF aerogels and CAs were investigated in detail by adjusting the amount of glycidol and water.

2 Experimental

2.1 Preparation of glycidol-catalyzed RF aerogels and CAs

R (~98%, TCI America), F (~38%, Sigma aldrich) and glycidol (~96%, Acros) were all used as received.

The synthesis methods of RF aerogels and CAs have been detailed described in our previous studies.[3] In this study, the synthetic scheme and preparation parameters of RF aerogels and CAs are shown in Fig. 1 and Table 1. Briefly, the R was dissolved into the F and the deioned water was added into the R–F solution to obtain the mixture solution of R and F with the continuous stirring of magnetic stirrer. The wet RF gels were obtained by adding the glycidol into the mixture solution of R and F. The organic RF aerogels were prepared by aging, solvent-exchange and drying of the wet RF gels. Then, the CAs were prepared by pyrolyzing of the organic RF aerogels at 900 °C under a N_2 atmosphere. In order to investigate the effect of concentration of glycidol on the properties of RF aerogels and CAs. The molar ratio of R and F were set to 1/2, the amount of glycidol was set to 1, 2 and 3 ml while the amount of water was set to 10, 15 and 20 ml, respectively. The obtained samples were named S1–S5 referred to the concentration of glycidol of 7.58%, 5.50%, 4.31%, 8.27% and 11.91%, which can be calculated by $V\% = \frac{V_{\text{glycidol}}}{V_{\text{glycidol}} + V_{\text{water}} + V_{\text{Formaldehyde}}}$ respectively.

2.2 Characterization of glycidol-catalyzed RF and carbon aerogels

Scanning electron microscopy (SEM, Hitachi S-4300) was used to characterize the microstructure of RF aerogels and CAs. The powder of RF aerogels and CAs were put to conductive carbon adhesive tabs and mounted on aluminium sample stubs. A 5 kV electron beam current was applied and images taken at 40 000 magnification. The composition of RF aerogels and CAs was measured by the X-ray diffraction (XRD, Rigaku Ultima III, Cu $K\alpha$ radiation, $\lambda = 1.54056$ Å, scanning rate: 2θ min^{-1}) and Fourier transform infrared spectroscopy (FTIR, Shimadzu 8400 s, collected at room temperature from 400 to 4000 cm^{-1}). After degassing for 24 h at 60 °C and 75 mmHg, the Specific Surface Area and Porosity Analyzer (Quantachrome Autosorb-iQ, software: ASiQwin 3.01) was used to determine nitrogen

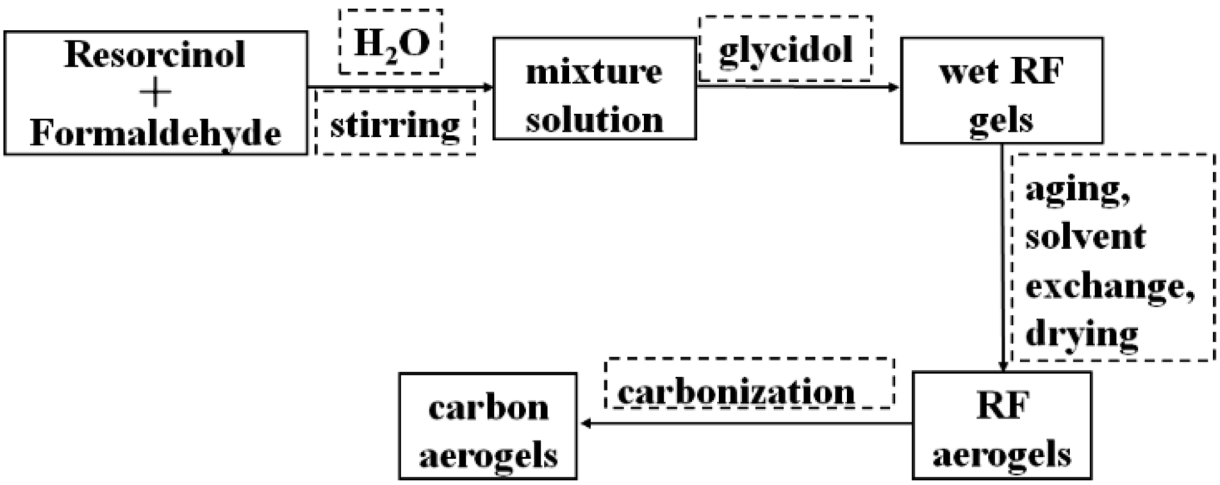

Fig. 1 Synthetic scheme of RF aerogels and Cas.

Table 1 Preparation parameters, color and densities of RF aerogels and CAs

Sample	R (g)	F (ml)	H_2O (ml)	Glycidol (ml)	V% (glycidol)	Color of RF aerogels	Density-RF (mg cm^{-3})	Density-CAs (mg cm^{-3})
S1	1.24	2.18	10	1	7.58	Reddish brown	190	195
S2	1.24	2.18	15	1	5.50	Orange	149	130
S3	1.24	2.18	20	1	4.31	Light orange	380	222
S4	1.24	2.18	20	2.00	8.27	Orange	107	112
S5	1.24	2.18	20	3.00	11.91	Reddish brown	96	110

adsorption/desorption isotherms and textural properties of RF aerogels and CAs at 77 K. The Brunauer–Emmett–Teller method was used to analyze BET surface areas (S_{BET}), micro-pore surface areas (S_{mic}) and micropore volume (V_{mic}) were obtained by t-plot method.

The residual dye concentration was measured by a Lambda 1050 UV/Vis/NIR (PerkinElmer, UK) spectrometer. The adsorption experiments of the glycidol-catalyzed CAs(S1–S5) for the removal of Rhodamine B (RhB) were conducted at room temperature. In order to investigate the evolution of solution concentration of RhB on adsorbent mass (CAs(S1–S5)), the CAs(S1–S5) were gradually added to 20 ml aqueous solution of RhB (25 mg L^{-1}) with the dose of 1 mg. The mixture was stirred for 240 min to ensure dispersion of the CAs(S1–S5) and allowed without disturbance for 240 min. the concentration of the filtered RhB solutions were measured by a UV-vis absorption spectrophotometer at 552 nm, and the removal rate of CAs(S1–S5) on RhB can be calculated by $(C_0–C_e)/C_0$, where C_0 and C_e are the initial and equilibrium solution concentration of RhB, respectively.

3 Results and discussion

3.1 Color and mass density of glycidol-catalyzed RF aerogels and CAs

The preparation parameters of RF aerogels and CAs were listed in Table 1 and its samples were denoted as S1–S5 which referred to the concentration of glycidol of 7.58%, 5.50%, 4.31%, 8.27% and 11.91%, respectively. Fig. 2(a–e) and Fig. 2(f–j) show the photographs of RF aerogels and corresponding CAs of S1–S5, respectively. The RF aerogels and CAs are both free-standing monolithic materials without any visible defects. The RF aerogels (Fig. 2(a) and (e)) are deep reddish brown and the RF aerogels (Fig. 2(b–d)) are orange, whereas their corresponding CAs (Fig. 2(f–j)) are black. It is worth noting that the color of RF aerogels (Fig. 2(a), (b) and (c)) changes from a deep reddish brown to light orange which is due to increasing the amount of water (10, 15 and 20 ml), and the color of RF aerogels (Fig. 2(c), (d) and (e)) has the reverse trend from light orange to reddish brown with increasing the amount of glycidol (1, 2 and 3 ml). Ultimately in both cases when the concentration of glycidol is decreased with respect to water, the resultant RF aerogels are lighter in color, which is agreement with the RF aerogels catalyzed by sodium carbonate.[45]

As described by Maldonado-Hódar *et al.*, the color of RF aerogels strongly depended on the concentration of catalyst (*e.g.* Na_2CO_3). For the case of higher catalyst concentration, the as-prepared RF aerogels displayed dark red color which indicated the polymerization of the R and F was complete. Reversely, for the case of lower catalyst concentration, the as-prepared RF aerogels of orange color indicated the polymerization of the R and F was not complete.[46] In this study, the changing color of the RF aerogels prepared by using glycidol as catalyst correlates to altering the level of polymerization of the R and F inside the RF aerogels, the RF aerogels with the darker color have undergone a higher level of polymerization compared those that exhibit the lighter orange tones, it can be concluded that the level of polymerization of R and F increases with the increasing of glycidol concentration.

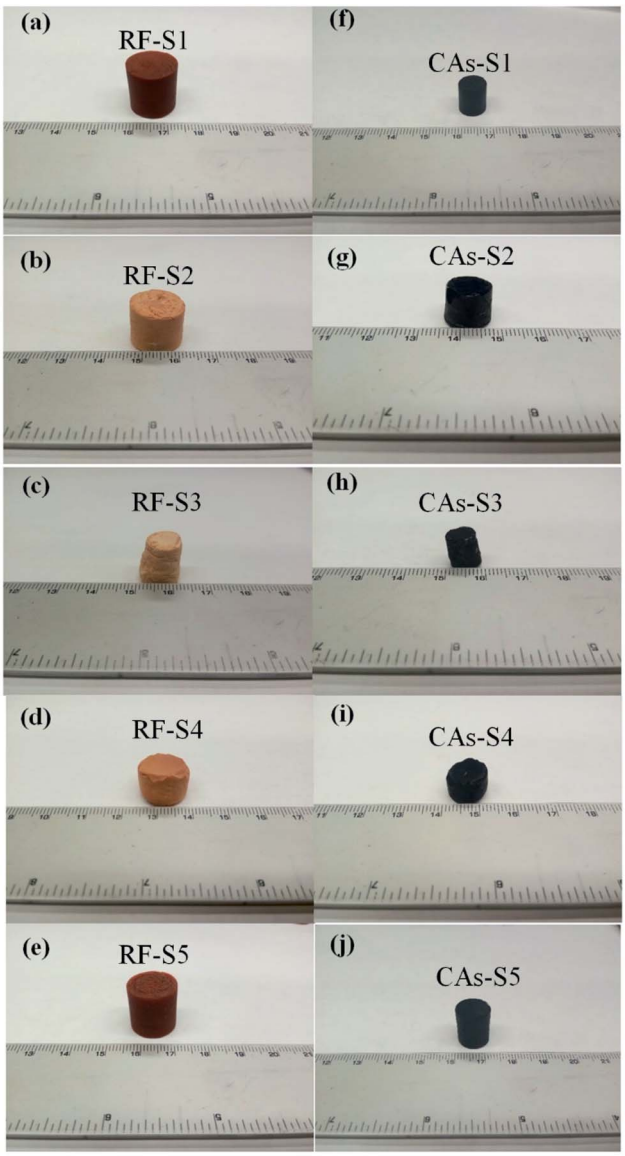

Fig. 2 Photographs of (a)–(e) RF aerogels and (f)–(j) CAs.

The density of RF aerogels and CAs changed a lot during the process of drying and carbonization, which can be attributed to the shrinkage of volume and evolving volatile of organic components. The RF aerogel (Fig. 2(c)) displayed the largest degree of shrinkage which is likely due to the lowest level of polymerization of the R and F, which results in highest density of RF aerogel and CAs. It can be seen from the Table 1 that the maximum densities of RF aerogels and CAs (located at S3) are 380 and 222 mg cm^{-3} while the minimum densities of RF aerogels and CAs (S5) are 96 and 110 mg cm^{-3}, which means the RF aerogels and CAs prepared by using glycidol as catalyst are low density materials and can be modified by adjusting the amount of glycidol and water.

3.2 Morphology and textual characteristics of glycidol-catalyzed RF aerogels and CAs

The microstructure of the RF aerogels and CAs were analyzed by SEM. Fig. 3(a–e) and Fig. 3 (f–j) show the SEM photographs of RF aerogels and corresponding CAs of S1–S5, respectively. As shown in Fig. 3(a–j), the RF aerogels and CAs are composed of "bead-like" 3-D networks of interconnected particles. The diameter of the particles of RF aerogels (Fig. 3(a–e)) and CAs (Fig. 3(f–j)) increase with the increasing of the amount of water (S1–S3) and decrease with the increasing of the amount of glycidol (S3–S5). The diameter of particles of RF aerogels ranges from several tens nanometers to several hundred nanometers, some spherical particles with the diameter of ~1 micron can be seen in Fig. 3(c) and (d), while the diameter of particles of CAs ranges from a few nanometers to several tens nanometers and there is no particle with the diameter larger than ~1 micron.

It is obvious that the level of polymerization of the R and F inside the RF aerogels plays a key role to the homogeneity of the particles of RF aerogels and CAs. The reddish brown RF aerogels with higher level of polymerization of the R and F lead to higher homogeneity of the particles of RF aerogels (Fig. 3(a) and (e)) and CAs (Fig. 3(f) and (j)) while the orange or light orange RF aerogels with lower level of polymerization of the R and F lead to lower homogeneity of the particles of RF aerogels (Fig. 3(b)–(d)) and CAs(Fig. 3(g)–(i)). Compared to the lower level of polymerization of the R and F inside the RF aerogels (Fig. 3(b)–(d)), the higher level of polymerization of the R and F inside the RF aerogels (Fig. 3(a) and (e)) facilitates to form a web-like nano structure rather than an accumulation of nanoparticles, which lead to lower shrinkage and higher mechanical properties. Additionally, compared to the corresponding CAs (Fig. 3(f) and (j)), the higher level of polymerization of the R and F inside the RF aerogels (Fig. 3(a) and (e)) lead to the increasing of the size of particles and reducing of the size of pores after a 900 °C annealing. Reversely, compared to the corresponding CAs (Fig. 3(g)–(i)), the lower level of polymerization of the R and F inside the RF aerogels (Fig. 3(b)–(d)) lead to the reducing of the size of particles and increasing of the size of pores after a 900 °C annealing.

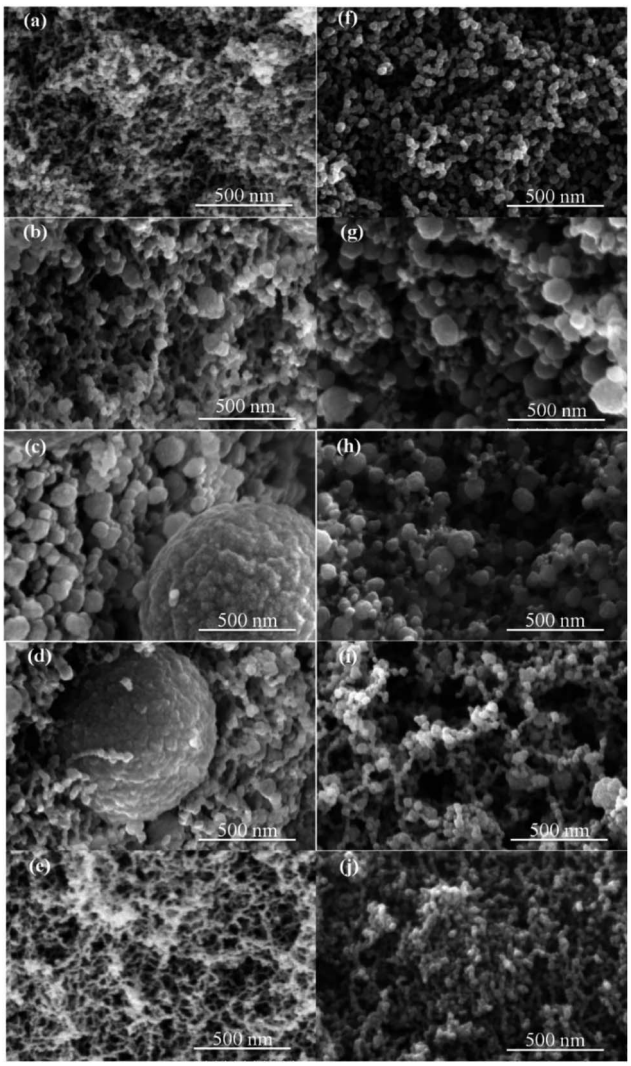

Fig. 3 SEM photographs of RF aerogels ((a)–(e)) and corresponding CAs ((f)–(j)) of S1–S5.

These results indicate that the diameter of particles and pores of RF aerogels and CAs can be adjusted by the amount of water and/or glycidol. The SEM images also show that the RF aerogels and CAs have a high porosity with pores ranging from micropores to macropores.

To further confirm the textual characteristics of RF aerogels and CAs, the Nitrogen adsorption/desorption isotherms analysis was performed on the RF aerogels and CAs to determine the BET specific surface area, micropore surface area, micropore volume, total pore volume and average pore size, which are summarized in Table 2. The results reveal that the concentration of glycidol have a significant impact on the S_{BET}, S_{mic} and V_{tot} of the RF aerogels. The S_{BET}, S_{mic} and V_{tot} of RF aerogels decrease with the increasing amount of water and increase with the increasing amount of glycidol. Due to the lowest level of polymerization of the R and F of RF-S3, it displays the lowest S_{BET} (70 $m^2\ g^{-1}$), S_{mic} (0 $m^2\ g^{-1}$) and highest D_{avg} (7.2 nm). Conversely, RF-S5 possesses the highest S_{BET} (291 $m^2\ g^{-1}$), S_{mic} (36 $m^2\ g^{-1}$) and lowest D_{avg} (4.7 nm) because of the highest level of polymerization of the R and F. The results of V_{mic} suggests the V_{mic} has negligible contribution to the V_{tot} of RF aerogels.

For the CAs, it is obviously observed that the carbonization of RF aerogels results in the remarkable improvement of S_{BET}, S_{mic}, V_{mic}/V_{tot} and significant reduction of D_{avg}, which could be ascribed to the evolving volatile of organic components of RF aerogels during the pyrolysis process and the generation of micropores (as shown in Fig. S1†). The maximum S_{BET} and S_{mic} are 597 (CAs-S5) and 443(CAs-S2) $m^2\ g^{-1}$ while the minimum S_{BET} and S_{mic} are 578 (CAs-S1) and 285 (CAs-S5) $m^2\ g^{-1}$, respectively. It is worth noting that the V_{mic}/V_{tot} of CAs-S2 (40.5%), CAs-S3 (34.9%) and CAs-S4 (22.5%) are much higher than that of CAs-S1 (15.0%) and CAs-S5 (17.7%), indicating that the RF aerogels with lower level of polymerization produce more micropores during the process of carbonization.

Therefore, the higher the concentration of glycidol, the higher the level of polymerization of R and F is, and the higher

Table 2 Textual characteristics of glycidol-catalyzed RF aerogels and Cas[a]

Samples	S_{BET} (m^2 g^{-1})	S_{mic} (m^2 g^{-1})	V_{tot} (cm^3 g^{-1})	V_{mic} (cm^3 g^{-1})	V_{mic}/V_{tot} (%)	D_{avg} (nm)
RF-S1	260	28	0.7	0	0	5.7
RF-S2	73	6	0.2	0	0	5.3
RF-S3	70	0	0.3	0	0	7.2
RF-S4	163	14	0.5	0	0	5.5
RF-S5	291	36	0.7	0	0	4.7
CAs–S1	578	304	0.9	0.1	15.0	2.9
CAs–S2	561	443	0.4	0.2	40.5	1.5
CAs–S3	554	410	0.5	0.2	34.9	1.7
CAs–S4	570	376	0.6	0.2	22.5	2.1
CAs–S5	597	285	0.7	0.1	17.7	2.3

[a] S_{BET} = BET surface area; S_{mic} = micropore surface area by t-method; V_{tot} = total pore volume; V_{mic} = micropore volume by t-method; D_{avg} = average pore size.

the S_{BET} of RF aerogels and CAs are. The size of the particles and pores of RF aerogels and CAs can be easily manipulated by adjusting the amount of water and glycidol to produce low density and high porosity materials.

3.3 Composition and sol-gel mechanisms of glycidol-catalyzed RF aerogels and CAs

The Fourier transform infrared spectroscopy (FTIR) of the resulting RF aerogels (S1–S5) and corresponding CAs are shown in Fig. 4(a) and (b). The FTIR spectra (Fig. 4(a)) shows the vibrational bands of various functional groups of RF aerogels: a broad peak at around 3400 cm^{-1} is ascribed to O–H stretching vibration from the physically adsorbed water molecule or hydroxyl groups on the surface of RF aerogels; the peaks located at ~2937 and ~1475 cm^{-1} are the asymmetric and symmetric C–H stretching vibrations; the peak at ~2380 cm^{-1} shows the stretching vibration of C–H bonds; the peak located at ~1609 cm^{-1} associated with the skeleton vibration of aromatic C=C bonds; the weak peak located at ~1374 cm^{-1} is the deformation mode of the C–H bonds; the appearing peaks at ~1221 and ~1095 cm^{-1} indicate the C–O–C stretching vibrations of methylene ether bridges between resorcinol molecules.

It is known to us that the glycidol consists of epoxide and hydroxyl groups and can react with the opening of the epoxy ring or its preservation.[47] According to the reported results of Tarnacka *et al.*, the characteristic peaks of the vibration of C–O–C in epoxide ring of glycidol can be observed in the 760–880 cm^{-1}.[48] However, no obvious peaks have been observed in the 760–880 cm^{-1} of RF aerogels (S1–S5), which means the sol-gel mechanism of glycidol-catalyzed RF aerogels may be the opening of epoxy ring rather than the preservation of epoxy ring. In the mixture of R and F, the proton (H^+ ion) was quickly consumed by the ring-opening reaction of epoxy group of glycidol and triggered the polymerization of R and F to form RF wet gels.[3] The by-products of the ring-opening reaction of glycidol was completely exchanged during the process of solvent-exchange and CO_2 supercritical drying.

Fig. 4(b) shows the FTIR spectra of CAs. The intensities of the adsorption peaks of the CAs have an obviously reduction after the carbonization of RF aerogels at 900 °C under the protection of N_2 atmosphere. The reduction (or disappearing) of C–O–C (at ~1221 and ~1095 cm^{-1}) and C–H peak intensities in the spectra of CAs implies the completely decomposition of RF aerogels and the formation of amorphous carbon, this is also confirmed by XRD analysis results illustrated in Fig. 5.

Fig. 5 shows the XRD diffraction pattern of RF aerogels (S5) and CAs(S5) and these patterns are representative of the other RF aerogels and CAs. The results indicate that both the RF

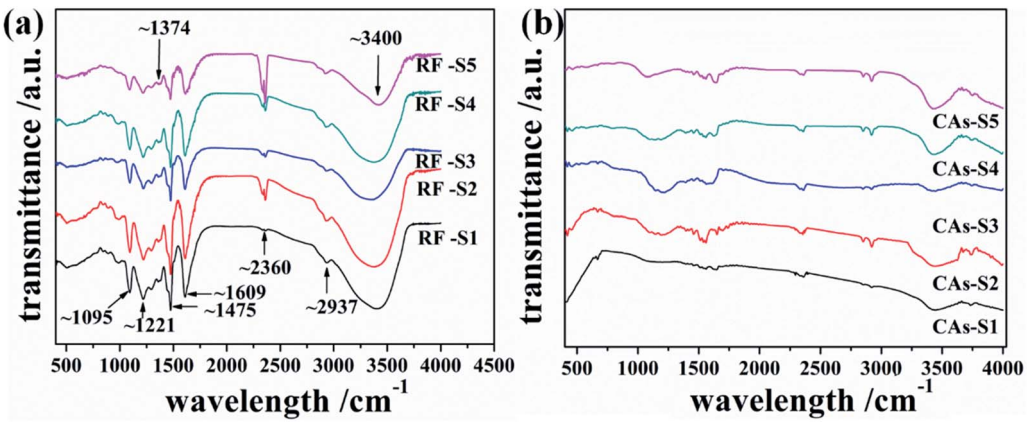

Fig. 4 FTIR spectra of (a) RF aerogels and (b) CAs.

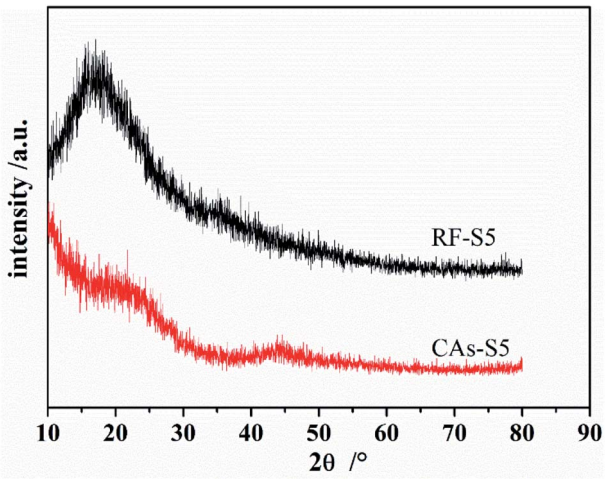

Fig. 5 XRD of RF aerogels and CAs.

aerogels and CAs are highly amorphous materials showing no crystalline structure. Considering the results derived from FTIR transmittance spectra, no obvious shifting of peaks or other impurity phase in the final product indicate that RF aerogels can be completely converted to CAs after a 900 °C pyrolysis under the protection of N_2 atmosphere.

3.4 Adsorption properties of glycidol-catalyzed CAs

CAs are widely used as adsorbents because of the characteristic of high surface area. The calibration curves of RhB and the influence of adsorbent dosage of CAs on removal rate of RhB is shown in Fig. 6, It is revealed that the removal efficiency of RhB increase linearly as increasing the absorbent dosage of CAs. However, the slopes of adsorption curves of CAs are significant different, which means the porosity of CAs plays a key role on the removal efficiency of RhB. In order to achieve ~100% of removal efficiency of RhB, the added doses of CAs(S1–S5) were 5, 10, 15, 6 and 4 mg, respectively. Considering the mass of RhB in the initial RhB solution, the adsorption capacity of CAs (S1–S5) can be calculated as 100, 50, 33, 83 and 125 mg g^{-1}, respectively, which are higher than that of some reported CAs catalyzed by base and acid catalysts.[49] The slopes of adsorption curves and adsorption capacity of CAs (S1, S5) are much higher than that of CAs (S2, S3 and S4), which can be directly correlated to the higher surface area, total pore volume and average pore size exhibited by these materials.

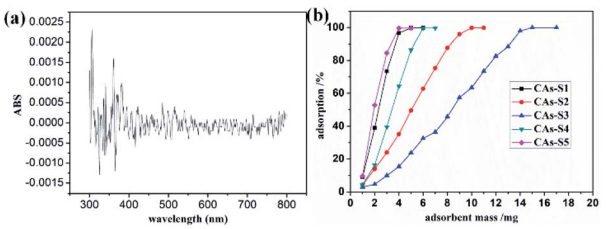

Fig. 6 (a) Calibration curves of RhB and (b) adsorption curves of CAs.

Conclusions

Glycidol, consists of an epoxy group and a hydroxyl group, are usually used as catalyst to prepare metal oxide aerogels. In this study, Glycidol was used to the synthesis of RF aerogels and CAs. The evolution of color, density, morphology, porosity and adsorption properties of the RF aerogels and CAs were investigated by adjusting the concentration of glycidol. With the increasing of glycidol concentration, the color of RF aerogels had the trends from light orange to dark reddish brown, which can be ascribed to the improvement of level of polymerization of the R and F inside the RF aerogels. No obvious peaks have been observed in the 760–880 cm^{-1} of RF aerogels, which means the sol-gel mechanism of glycidol-catalyzed RF aerogels is the opening of epoxy ring rather than the preservation of epoxy ring. The resultant CAs are low density (~96 mg cm^{-1-3}), high porosity (~597 m^2 g^{-1}) amorphous materials, which possess high adsorption capacity (~125 mg g^{-1}) on RhB. Moreover, this method may promote the successful synthesis of metal oxide doped CAs with interpenetrating networks and high crystallization nanoparticles.

Author contributions

Xiurong Zhu: conceptualization, methodology, investigation, writing original draft, supervision. Lousia J. Hope-Weeks: conceptualization, supervision, writing-review & editing. Yi Yu: funding acquisition, writing-review & editing. Jvjun Yuan: investigation, methodology, validation, formal analysis, visualization. Xianke Zhang: investigation, formal analysis, visualization. Huajun Yu: validation, formal analysis. Jiajun Liu: writing-review & editing. Xiaofen Li: writing-review & editing. Xianghua Zeng: writing-review & editing.

Conflicts of interest

The authors declare that they have no known competing financial interests or personal relationships that could have appeared to influence the work reported in this paper.

Acknowledgements

The authors gratefully acknowledge the Texas Tech University Imaging Center, Department of Biological Sciences, for use of the Hitachi S-4300; the authors also gratefully acknowledge the Department of Chemistry & Biochemistry at Texas Tech University for use of the Rigaku Ultima III X-ray powder diffractometer. The authors would also like to personally thank Dr Dominick J. Casadonte for use of Shimadzu 8400 s Fourier transform infrared spectrometer. This research was financially supported by the National Natural Science Foundation of China (No. 51762003, 11647101) and the Opening Project of Shanghai Key Laboratory of Special Artificial Microstructure Materials and Technology (ammt2017A-8), the authors are exceedingly grateful.

References

1 A. Du, B. Zhou, Z. Zhang and J. Shen, A Special Material or a New State of Matter: A Review and Reconsideration of the Aerogel, *Materials*, 2013, **6**, 941–968.

2 S. Z. Jiao, Z. C. Sun, J. Y. Wen, Y. Y. Liu, F. R. Li, Q. Q. Miao, W. X. Wu, L. H. Li and Y. Zhou, Development of Rapid Curing SiO2 Aerogel Composite-Based QuasiSolid-State Dye-Sensitized Solar Cells through Screen-Printing Technology, *ACS Appl. Mater. Interfaces*, 2020, **12**, 48794–48803.

3 Z. Xiurong, H.-W. J. Lousia, B. Roya, C. R. Vanessa, Y. Yi, Z. Lingwei, W. Xinghua, L. Dongbo and Z. Xianghua, Enhanced compressive strength of carbon aerogels with low density and high specific surface areas, *J. Porous Mater.*, 2022, DOI: **10.1007/s10934-022-01254-w**.

4 C. W. Wu, P. H. Li, Y. M. Wei, C. Yang and W. J. Wu, Review on the preparation and application of lignin-based carbon aerogels, *RSC Adv.*, 2022, **12**, 10755–10765.

5 E. Garcia-Bordeje, A. M. Benito and W. K. Maser, Graphene aerogels *via* hydrothermal gelation of graphene oxide colloids: Fine-tuning of its porous and chemical properties and catalytic applications, *Adv. Colloid Interface Sci.*, 2021, 292.

6 P. Zhao, B. Jin, J. Yan and R. F. Peng, Fabrication of recyclable reduced graphene oxide/graphitic carbon nitride quantum dot aerogel hybrids with enhanced photocatalytic activity, *RSC Adv.*, 2021, **11**, 35147–35155.

7 V. Agarwal, N. Varghese, S. Dasgupta, A. K. Sood and K. Chatterjee, Engineering a 3D MoS2 foam using keratin exfoliated nanosheets, *Chem. Eng. J.*, 2019, **374**, 254–262.

8 R. W. Pekala, Organic Aerogels from the Polycondensation of Resorcinol with Formaldehyde, *J. Mater. Sci.*, 1989, **24**, 3221–3227.

9 R. W. Pekala, J. C. Farmer, C. T. Alviso, T. D. Tran, S. T. Mayer, J. M. Miller and B. Dunn, Carbon aerogels for electrochemical applications, *J. Non-Cryst. Solids*, 1998, **225**, 74–80.

10 W. J. Yuan, C. J. Hou, X. L. Zhang, S. X. Zhong, Z. J. Luo, D. C. Mo, Y. F. Zhang and X. W. Liu, Constructing a Cathode Catalyst Layer of a Passive Direct Methanol Fuel Cell with Highly Hydrophilic Carbon Aerogel for Improved Water Management, *ACS Appl. Mater. Interfaces*, 2019, **11**, 37626–37634.

11 Z. Zhang, S. Zhao, G. B. Chen, K. F. Li, Z. F. Fei, Z. Y. Luo and Z. C. Yang, Progress on Carbon Aerogels as the Supports of Fuel Cell Catalysts, *Rare Met. Mater. Eng.*, 2020, **49**, 3977–3986.

12 A. Arenillas, J. A. Menendez, G. Reichenauer, A. Celzard, V. Fierro, F. J. M. Hodar, E. Bailon-Garcia and N. Job, Properties of Carbon Aerogels and Their Organic Precursors, *Adv. Sol. Der. Mat. Tech.*, 2019, 87–121.

13 F. Yang, L. L. Sun, W. L. Xie, Q. Jiang, Y. Gao, W. Zhang and Y. Zhang, Nitrogen-functionalization biochars derived from wheat straws *via* molten salt synthesis: An efficient adsorbent for atrazine removal, *Sci. Total Environ.*, 2017, **607**, 1391–1399.

14 K. J. Wang, Z. W. Ye, X. Q. Li and J. N. Yang, Nanoporous resorcinol-formaldehyde based carbon aerogel for lightweight and tunable microwave absorption, *Mater. Chem. Phys.*, 2022, 278.

15 Y. L. Xu, B. Ren, S. S. Wang, L. H. Zhang and Z. F. Liu, Carbon aerogel-based supercapacitors modified by hummers oxidation method, *J. Colloid Interface Sci.*, 2018, **527**, 25–32.

16 M. Oschatz, S. Boukhalfa, W. Nickel, J. P. Hofmann, C. Fischer, G. Yushin and S. Kaskel, Carbide-derived carbon aerogels with tunable pore structure as versatile electrode material in high power supercapacitors, *Carbon*, 2017, **113**, 283–291.

17 L. Zhu, H. T. Jiang, W. X. Ran, L. J. You, S. S. Yao, X. Q. Shen and F. Y. Tu, Turning biomass waste to a valuable nitrogen and boron dual-doped carbon aerogel for high performance lithium-sulfur batteries, *Appl. Surf. Sci.*, 2019, **489**, 154–164.

18 F. Yu, X. C. Zhang, Z. Q. Yang, P. Y. Yang, L. Q. Li, J. Wang, M. T. Shi and J. Ma, Carbon aerogel electrode for excellent dephosphorization *via* flow capacitive deionization, *Desalination*, 2022, 528.

19 K. D. Wu, Q. Zhou, J. X. Cao, Z. Qian, B. Niu and D. H. Long, Ultrahigh-strength carbon aerogels for high temperature thermal insulation, *J. Colloid Interface Sci.*, 2022, **609**, 667–675.

20 S. Chandrasekaran, B. Yao, T. Y. Liu, W. Xiao, Y. Song, F. Qian, C. Zhu, E. B. Duoss, C. M. Spadaccini, Y. Li and M. A. Worsley, Direct ink writing of organic and carbon aerogels, *Mater. Horiz.*, 2018, **5**, 1166–1175.

21 S. J. Yuan, W. Fan, D. Wang, L. S. Zhang, Y. E. Miao, F. L. Lai and T. X. Liu, 3D printed carbon aerogel microlattices for customizable supercapacitors with high areal capacitance, *J. Mater. Chem. A*, 2021, **9**, 423–432.

22 B. Yao, H. R. Peng, H. Z. Zhang, J. Z. Kang, C. Zhu, G. Delgado, D. Byrne, S. Faulkner, M. Freyman, X. H. Lu, M. A. Worsley, J. Q. Lu and Y. Li, Printing Porous Carbon Aerogels for Low Temperature Supercapacitors, *Nano Lett.*, 2021, **21**, 3731–3737.

23 Y. Ge, T. Zhang, B. Zhou, H. Q. Wang, Z. H. Zhang, J. Shen and A. Du, Nanostructured resorcinol-formaldehyde ink for 3D direct writing, *J. Mater. Res.*, 2018, **33**, 2052–2061.

24 C. Moreno-Castilla and F. J. Maldonado-Hodar, Carbon aerogels for catalysis applications: An overview, *Carbon*, 2005, **43**, 455–465.

25 I. D. Alonso-Buenaposada, N. Rey-Raap, E. G. Calvo, J. A. Menendez and A. Arenillas, Acid-based resorcinol-formaldehyde xerogels synthesized by microwave heating, *J. Sol-Gel Sci. Technol.*, 2017, **84**, 60–69.

26 A. Arenillas, J. A. Menendez, G. Reichenauer, A. Celzard, V. Fierro, F. J. M. Hodar, E. Bailon-Garcia and N. Job, Organic and Carbon Gels: From Laboratory to Industry?, *Adv Sol Der Mat Tech*, 2019, 1–26.

27 A. P. Pandey, A. Bhatnagar, V. Shukla, P. K. Soni, S. Singh, S. K. Verma, M. Shaneeth, V. Sekkar and O. N. Srivastava,

Hydrogen storage properties of carbon aerogel synthesized by ambient pressure drying using new catalyst triethylamine, *Int. J. Hydrogen Energy*, 2020, **45**, 30818–30827.

28 S. H. Inn, J. C. Jung and M. S. Kim, Pore Structure and Electrochemical Properties of Carbon Aerogels as an EDLC-Electrode with Different Preparation Conditions, *Korean J. Mater. Res.*, 2018, **28**, 50–61.

29 M. Alam, S. A. Mirbagheri and M. R. Ghaani, Multi-parameter optimization of the capacitance of Carbon Xerogel catalyzed by NaOH for application in supercapacitors and capacitive deionization systems, *Heliyon*, 2019, **5**, DOI: **10.1016/j.heliyon.2019.e01196**.

30 T. Horikawa, J. i. Hayashi and K. Muroyama, Size control and characterization of spherical carbon aerogel particles from resorcinol–formaldehyde resin, *Carbon*, 2004, **42**, 169–175.

31 M. F. Yan, L. H. Zhang, R. He and Z. F. Liu, Synthesis and characterization of carbon aerogels with different catalysts, *J. Porous Mater.*, 2015, **22**, 699–703.

32 D. Fairen-Jimenez, F. Carrasco-Marin and C. Moreno-Castilla, Adsorption of benzene, toluene, and xylenes on monolithic carbon aerogels from dry air flows, *Langmuir*, 2007, **23**, 10095–10101.

33 M. R. Sala, S. Chandrasekaran, O. Skalli, M. Worsley and F. Sabri, Enhanced neurite outgrowth on electrically conductive carbon aerogel substrates in the presence of an external electric field, *Soft Matter*, 2021, **17**, 4489–4495.

34 I. Najeh, N. Ben Mansour, M. Mbarki, A. Houas, J. P. Nogier and L. El Mir, Synthesis and characterization of electrical conducting porous carbon structures based on resorcinol-formaldehyde, *Solid State Sci.*, 2009, **11**, 1747–1751.

35 A. Mohammad, A. Kareem, A. U. Mirza, S. A. Bhat, S. A. A. Nami, S. Rehman and N. Nishat, Enhanced performance of terpolymer resin derived from resorcinol/formaldehyde/salicylic acid for antibacterial application, *Int. J. Ind. Chem.*, 2020, **11**, 235–248.

36 J. Laskowski, B. Milow and L. Ratke, Subcritically dried resorcinol–formaldehyde aerogels from a base–acid catalyzed synthesis route, *Microporous Mesoporous Mater.*, 2014, **197**, 308–315.

37 A. A. Mahani, S. Motahari and V. Nayyeri, Synthesis, characterization and dielectric properties of one-step pyrolyzed/activated resorcinol-formaldehyde based carbon aerogels for electromagnetic interference shielding applications, *Mater. Chem. Phys.*, 2018, **213**, 492–501.

38 S. Gunes and C. Guldur, Synthesis of large pore sized ordered mesoporous carbons using triconstituent self-assembly strategy under different acidic conditions and ratios of carbon precursor to structure directing agent, *Colloid Polym. Sci.*, 2018, **296**, 799–807.

39 J. B. Wang, X. Q. Yang, D. C. Wu, R. W. Fu, M. S. Dresselhaus and G. Dresselhaus, The porous structures of activated carbon aerogels and their effects on electrochemical performance, *J. Power Sources*, 2008, **185**, 589–594.

40 Y. L. Xu, M. F. Yan, S. S. Wang, L. H. Zhang, H. H. Liu and Z. F. Liu, Synthesis, characterization and electrochemical properties of carbon aerogels using different organic acids as polymerization catalysts, *J. Porous Mater.*, 2017, **24**, 1375–1381.

41 J. Choma, K. Jedynak, M. Marszewski and M. Jaroniec, Organic acid-assisted soft-templating synthesis of ordered mesoporous carbons, *Adsorption*, 2013, **19**, 563–569.

42 D. C. Wu, R. W. Fu, S. T. Zhang, M. S. Dresselhaus and G. Dresselhaus, Preparation of low-density carbon aerogels by ambient pressure drying, *Carbon*, 2004, **42**, 2033–2039.

43 S. A. Al-Muhtaseb and J. A. Ritter, Preparation and Properties of Resorcinol–Formaldehyde Organic and Carbon, *Gels*, 2003, **15**, 101–114.

44 A. M. ElKhatat and S. A. Al-Muhtaseb, Advances in Tailoring Resorcinol-Formaldehyde Organic and Carbon Gels, *Adv. Mater.*, 2011, **23**, 2887–2903.

45 R. A. Fonseca-Correa, L. Giraldo and J. C. Moreno-Pirajan, Thermodynamic study of adsorption of nickel ions onto carbon aerogels, *Heliyon*, 2019, **5**, e01789.

46 F. J. Maldonado-Hódar, M. A. Ferro-García, J. Rivera-Utrilla and C. Moreno-Castilla, Synthesis and textural characteristics of organic aerogels, transition-metal-containing organic aerogels and their carbonized derivatives, *Carbon*, 1999, **37**, 1199–1205.

47 A. W. Anna Fajdek and E. Milchert, Significance and use of glycidol, *Chemik*, 2010, **64**, 1–5.

48 M. Tarnacka, T. Flak, M. Dulski, S. Pawlus, K. Adrjanowicz, A. Swinarew, K. Kaminski and M. Paluch, High pressure polymerization of glycidol. Kinetics studies, *Polymer*, 2014, **55**, 1984–1990.

49 M. Ptaszkowska-Koniarz, J. Goscianska and R. Pietrzak, Removal of rhodamine B from water by modified carbon xerogels, *Colloids Surf., A*, 2018, **543**, 109–117.